Article

High-performing polysulfate dielectrics for electrostatic energy storage under harsh conditions

He Li, Boyce S. Chang, Hyunseok Kim, ..., K. Barry Sharpless, Peng Wu, Yi Liu

sharples@scripps.edu (K.B.S.)
pengwu@scripps.edu (P.W.)
yliu@lbl.gov (Y.L.)

Highlights

Polysulfates are revealed as excellent dielectric materials for the first time

Polysulfate-based film capacitors deliver superior energy density under high heat

Coating of ultrathin Al_2O_3 nanolayers increases energy storage capacity

The high fidelity "click" synthesis sets the stage for more robust dielectrics

Based off a near-perfect click chemistry reaction—sulfur(VI) fluoride exchange (SuFEx) catalysis, flexible sulfate linkages are "clicked" with rigid aromatic ring systems to yield high-performing polysulfate dielectrics. Polysulfates exhibit features such as electrically insulating, mechanically flexible, and thermally stable, all being essential for their utilization in high-temperature dielectric film capacitors. Upon coating of ultrathin Al_2O_3 layers on polymer films, the polysulfate-based capacitors display superior electrostatic energy storage performance operating under thermal and electrical extremes ($\geq 150°C$ and 750 MV/m).

Article

High-performing polysulfate dielectrics for electrostatic energy storage under harsh conditions

He Li,[1,2,9] Boyce S. Chang,[2,9,10] Hyunseok Kim,[3] Zongliang Xie,[5] Antoine Lainé,[1] Le Ma,[1,6] Tianlei Xu,[5] Chongqing Yang,[2] Junpyo Kwon,[1,7] Steve W. Shelton,[2] Liana M. Klivansky,[2] Virginia Altoé,[2] Bing Gao,[3] Adam M. Schwartzberg,[2] Zongren Peng,[5] Robert O. Ritchie,[1,6,7] Ting Xu,[1,6,8] Miquel Salmeron,[1,6] Ricardo Ruiz,[2] K. Barry Sharpless,[3,*] Peng Wu,[4,*] and Yi Liu[1,2,11,*]

SUMMARY

High-capacity polymer dielectrics that operate with high efficiencies under harsh electrification conditions are essential components for advanced electronics and power systems. It is, however, fundamentally challenging to design polymer dielectrics that can reliably withstand demanding temperatures and electric fields, which necessitate the balance of key electronic, electrical, and thermal parameters. Herein, we demonstrate that polysulfates, synthesized by sulfur(VI) fluoride exchange (SuFEx) catalysis, another near-perfect click chemistry reaction, serve as high-performing dielectric polymers that overcome such bottlenecks. Free-standing polysulfate thin films from convenient solution processes exhibit superior insulating properties and dielectric stability at elevated temperatures, which are further enhanced when ultrathin (∼5 nm) oxide coatings are deposited by atomic layer deposition. The corresponding electrostatic film capacitors display high breakdown strength (>700 MV m^{-1}) and discharged energy density of 8.64 J cm^{-3} at 150°C, outperforming state-of-the-art free-standing capacitor films based on commercial and synthetic dielectric polymers and nanocomposites.

INTRODUCTION

Innovative dielectric materials that store energy with high efficiency and operate robustly under elevated temperatures and high electric field conditions are indispensable for rapidly advancing electrification in electronics and power systems.[1–4] While polymer-based dielectrics exhibit intrinsic characteristics of lightweight,[4–7] greater processability,[7,8] flexibility,[4–11] and voltage tolerance capability[4–11] compared with inorganic dielectric ceramics,[12–14] achieving simultaneous electrical and thermal endurance has been an outstanding challenge for their industrial applications in electric vehicles (EVs), avionics, space and underground oil and gas explorations.[15–17] For high-capacity electrostatic energy storage, polymer dielectrics with both high dielectric constant (k) and high dielectric breakdown strength (E_b) are desired, as the stored energy density of a linear dielectric material is proportional to the k and the square of E_b.[15–17] In addition to energy density, charge-discharge efficiency (η) is another essential performance factor for practical electrostatic energy storage. At elevated temperatures, both E_b and η are adversely impacted and may drop precipitously.[15–17] Such temperature-limited performance dependence is exemplified by the electrostatic film capacitors used in power inverters of

hybrid EVs. The benchmark dielectric polymer, biaxially oriented polypropylene (BOPP), is limited to operating temperatures below 105°C.[15] For its use in hybrid EVs, an accompanying cooling system is necessary to lower the working temperature from ~140°C to ~70°C in order to deliver a reliable energy storage performance, which adds extra mass and volume that compromise the energy efficiency of hybrid EVs.[15,17]

In the pursuit of reliable high-temperature dielectric polymers, the common strategy focuses on leveraging aromatic groups to offer polymers with a high glass transition temperature (T_g, i.e., ≥ 150°C), such as poly(ether ether ketone) (PEEK), polyetherimide (PEI), fluorene polyester (FPE), and polyimide (PI).[4,15–17] While thermomechanical stability can be satisfied in these high-T_g polymers, electrothermal stability remains poor under critical electric fields, even at operative temperatures way below their T_g. This liability is attributed primarily to the exponentially increased leakage current that is a universal problem across polymer dielectrics with rising temperature and electric field strength.[18,19] Consequently, when operating under high electric fields and elevated temperatures, the engineered high-T_g polymers usually display poor η, e.g., 37.1% for PEEK and 48.6% for FPE, at 150°C and 400 MV m^{-1}. Such performance deficits motivate the development of new polymer dielectrics that can achieve concurrent high energy density and high η at high temperatures. Large k, E_b, and T_g as well as low leakage currents are the linked properties that need to coexist in these polymers. Despite considerable efforts toward this end, as represented by dipolar glass polymers with high k values,[20–22] olefin-based polymers exhibiting large band gaps,[19,23,24] crosslinked fluoropolymers,[18] molecular semiconductor-doped polymers,[25] polymer blends,[26] and polymer-nanofiller composites,[4,27–29] balancing k, E_b and T_g remains a fundamental materials challenge since two or more of these parameters are mutually restrictive.

In this work, we report the discovery of polysulfates as a class of high-performing dielectrics exhibiting desirable k (3.4–3.8), high E_b (≥ 650 MV m^{-1}), and high T_g (153°C–225°C). This combination of physical characteristics endows aryloxy-polysulfate thin films with superior dielectric and energy storage properties at elevated temperatures, with notably higher energy density and efficiency than other state-of-the-art commercial dielectric polymers. Moreover, upon coating the film with nanometer layers of Al_2O_3, the E_b and electrostatic energy storage performance is further augmented, giving rise to a high discharged energy density (U_d) of 8.64 J cm^{-3} obtained at 750 MV m^{-1} and 150°C, which to the best of our knowledge, exceeds the performance of the known free-standing film-based dielectric polymers and nanocomposites.

RESULTS AND DISCUSSION

Materials design, synthesis, and characterization

For high-temperature applications of dielectric polymers, it is essential to possess a T_g above the operation temperature because drastically enhanced segmental motion of polymeric chains at temperatures close to T_g will result in significantly increased current leakage and reduced mechanical strength, and consequently deteriorated electrical insulation properties. It is equally important for the material to possess a wide band gap (E_g) to minimize electrical conduction within the polymer. Incorporating aromatic repeat units in the polymer backbone can effectively improve T_g but often reduces E_g due to conjugation effects of aromatic groups. Such an inverse T_g-E_g correlation has been commonly observed in conventional high-temperature polymers containing aromatic groups, rendering them unsuitable

[1]Materials Sciences Division, Lawrence Berkeley National Laboratory, Berkeley, CA 94720, USA

[2]The Molecular Foundry, Lawrence Berkeley National Laboratory, Berkeley, CA 94720, USA

[3]Department of Chemistry and The Skaggs Institute for Chemical Biology, The Scripps Research Institute, La Jolla, CA 92037, USA

[4]Department of Molecular Medicine, The Scripps Research Institute, La Jolla, CA 92037, USA

[5]State Key Laboratory of Electrical Insulation and Power Equipment, School of Electrical Engineering, Xi'an Jiaotong University, Xi'an 710049, Shaanxi, China

[6]Department of Materials Science and Engineering, University of California, Berkeley, Berkeley, CA 94720, USA

[7]Department of Mechanical Engineering, University of California, Berkeley, Berkeley, CA 94720, USA

[8]Department of Chemistry, University of California, Berkeley, Berkeley, CA 94720, USA

[9]These authors contributed equally

[10]Present address: Department of Materials Science and Engineering, Ames, IA 50010, USA

[11]Lead contact

*Correspondence: sharpless@scripps.edu (K.B.S.), pengwu@scripps.edu (P.W.), yliu@lbl.gov (Y.L.)
https://doi.org/10.1016/j.joule.2022.12.010

for high-temperature electrification applications. To address the constraints imposed by conjugation in polymeric materials, a strategy has been adopted to construct a fused bicyclic polyolefin-based aliphatic backbone while placing aromatic groups on the side chain, which realizes high performance dielectric polymers with high T_g and E_g.[19,23,24] Aside from the polyolefin system, effective approaches toward high-temperature dielectric polymers remain out of reach. Herein, we demonstrate that this dearth can be addressed by exercising simple yet powerful design considerations to mitigate the conjugation effect in the more common main-chain aromatic polymers. In particular, since the physical properties of polymers are dependent on the chemical nature of the linkage groups,[11,15,22,30] the employment of appropriate nonconjugated linkages between aromatic repeat units may impart a wide E_g while preserving the good thermal properties of aromatic polymers. In this regard, the highly stable and rotatable diaryl sulfate linkage stands out as a unique candidate. Compared with other common linkages such as imide, amide, ketone, ether, ester, and sulfone, the tetragonal sulfur(VI)-based sulfate functions as a nonplanar hub that connects the aromatic groups with interrupted conjugation and minimized π-π stacking, satisfying the E_g considerations. Additionally, the high polarizability and rotational freedom associated with the unconventional bonding characters of S(VI)=O and the S–O–C bonds in sulfate linkages are desirable to engender a reasonably high k value with synchronous low dielectric losses in main-chain polysulfates,[31] which is distinctive from side-chain dipolar polymers such as these bearing sulfonyl side groups.[21–23]

Nothing is known about the dielectric properties of main-chain polysulfates, however, presumably due to limited synthetic access to such polymers. Thanks to the recently discovered sulfur(VI) fluoride exchange (SuFEx) catalysis,[32–35] known as an emerging near-perfect and metal-free click chemistry reaction,[36,37] both sulfate linkages and aromatic groups can be readily incorporated into polymer backbones to afford main-chain polysulfates with extraordinary structural diversity and scalability (see experimental procedures and Figure 1A).[33–35] Out of a library of diaryl polysulfates prepared by SuFEx, three polymers (P1, P2, and P3, see Figure 1A) were selected for their varying T_g values (ranging from 153°C to 225°C) and high thermal decomposition temperatures ($T_{d95\%}$, defined as 5% weight loss, >350°C) (Figures S1–S4). The polysulfates display good solubility in conventional polar solvents such as N-methylpyrrolidone (NMP) and N,N-dimethylformamide (DMF) at room temperature, allowing the facile solution casting of flexible free-standing thin films that are desirable for practical electrostatic energy storage applications[30,38] (Figure S5).

All three polysulfates display desirable k values (e.g., 3.4–3.8 at 10^4 Hz) and low loss tangents (tan δ), as revealed by the frequency-dependent dielectric spectra (Figures 1B and S6). The experimental optical E_g values (obtained from UV-vis spectroscopy) are in the range between 4.36 and 3.90 eV and follow the order of P1 > P2 > P3, which agree favorably with the trend of the simulated electronic E_g values (obtained from density functional theory [DFT] calculations) (Figures 1C and S7–S9). When comparing the E_g and T_g values against the major commercial dielectric polymers containing aromatic repeat units, including PEEK, PEI, FPE, polyethylene terephthalate (PET), polyethylene naphthalate (PEN), polyamideimide (PAI), and PIs (Kapton PI and Upilex-S PI) (which follow an empirical inverse correlation between E_g and T_g), the polysulfates show an apparent deviation with decent T_g values despite their larger E_g values (Figures 1D and S10). In addition, the polysulfates P1–P3 display lower computed mass densities (~1.10–1.20 g cm^{-3}) than those of commercial dielectric polymers (Figure S11; Table S1). The combination of lightweight,
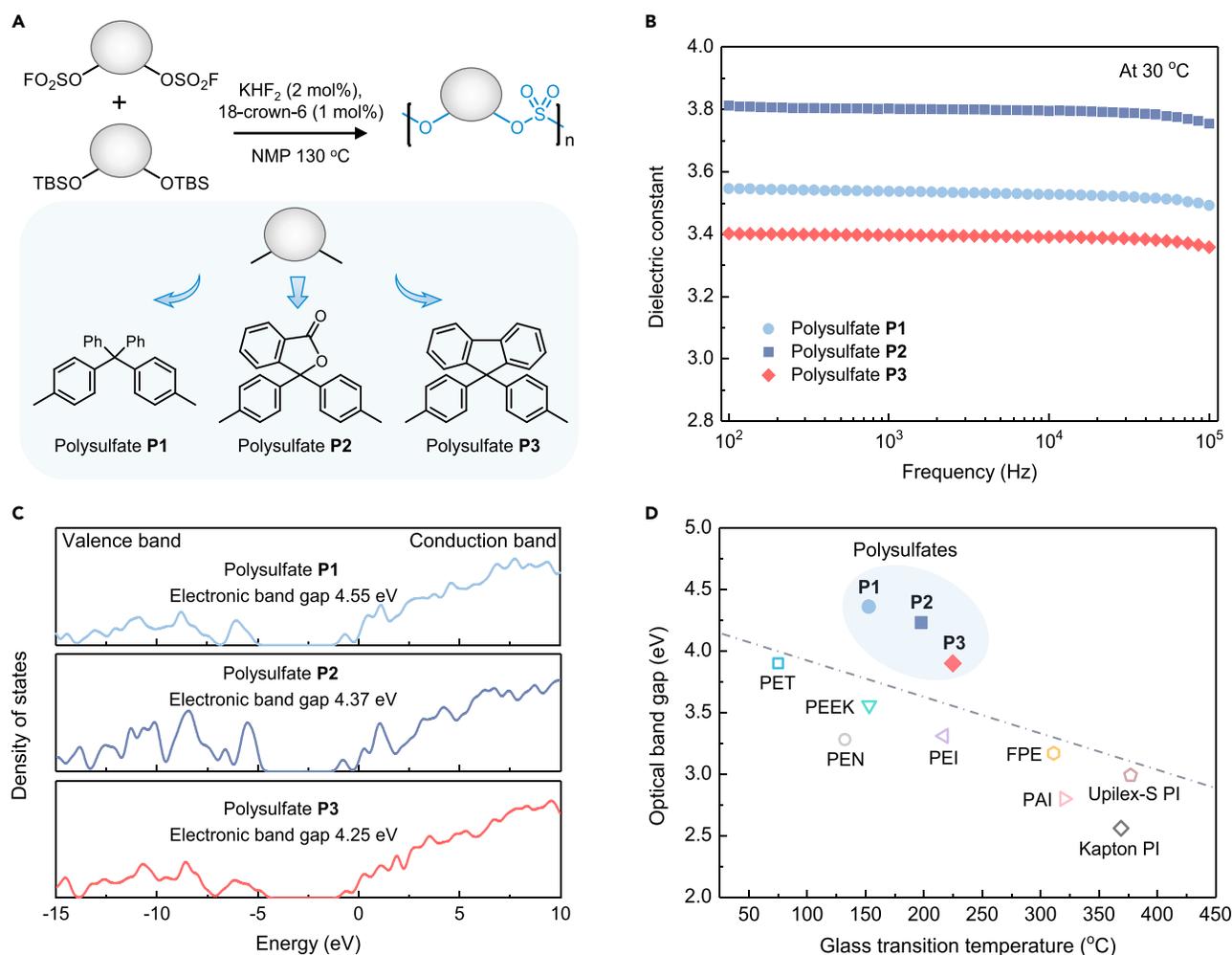
Figure 1. Chemical synthesis and electronic structure characterization

(A) Schematic of the polysulfates P1, P2, and P3 based on SuFEx click chemistry.

(B) Frequency-dependent dielectric spectra of dielectric constant (k) of polysulfates P1, P2, and P3 obtained at 30°C.

(C) Calculated density of states (DOS) and the corresponding computed electronic band gap of polysulfates P1, P2, and P3.

(D) Correlation between glass transition temperature and optical band gap of polysulfates P1, P2, and P3 and commercial aromatic dielectric polymers.[23]

wide E_g, large k, low tan δ, along with high T_g is likely essential for high-temperature film capacitor applications.

Temperature-dependent dielectric and electrostatic energy storage properties

To evaluate dielectric stability of polysulfates, the temperature-dependent dielectric spectra have been recorded across a wide temperature range and are shown in Figure S12. As the polysulfate P3 with the highest T_g also displays the most stable dielectric spectra up to 200°C, we compare the k and tan δ of polysulfate P3 with the state-of-the-art capacitor-grade polymer films, including BOPP, PEN, PEEK, PEI, FPE, Kapton PI, and Upilex-S PI (Table S2) as a function of temperature at 10^4 Hz (Figures 2A and 2B), which is the frequency of interest for common power conditioning.[4] The tan δ of polysulfate P3 is among the lowest (<0.2%) and even comparable to BOPP, which is known as the dielectric polymer with the smallest dielectric loss due to its non-polar structure. The ultra-low tan δ is attributable to the coexistence of the flexible sulfate linkages and the rigid aromatic subunits on the polymer
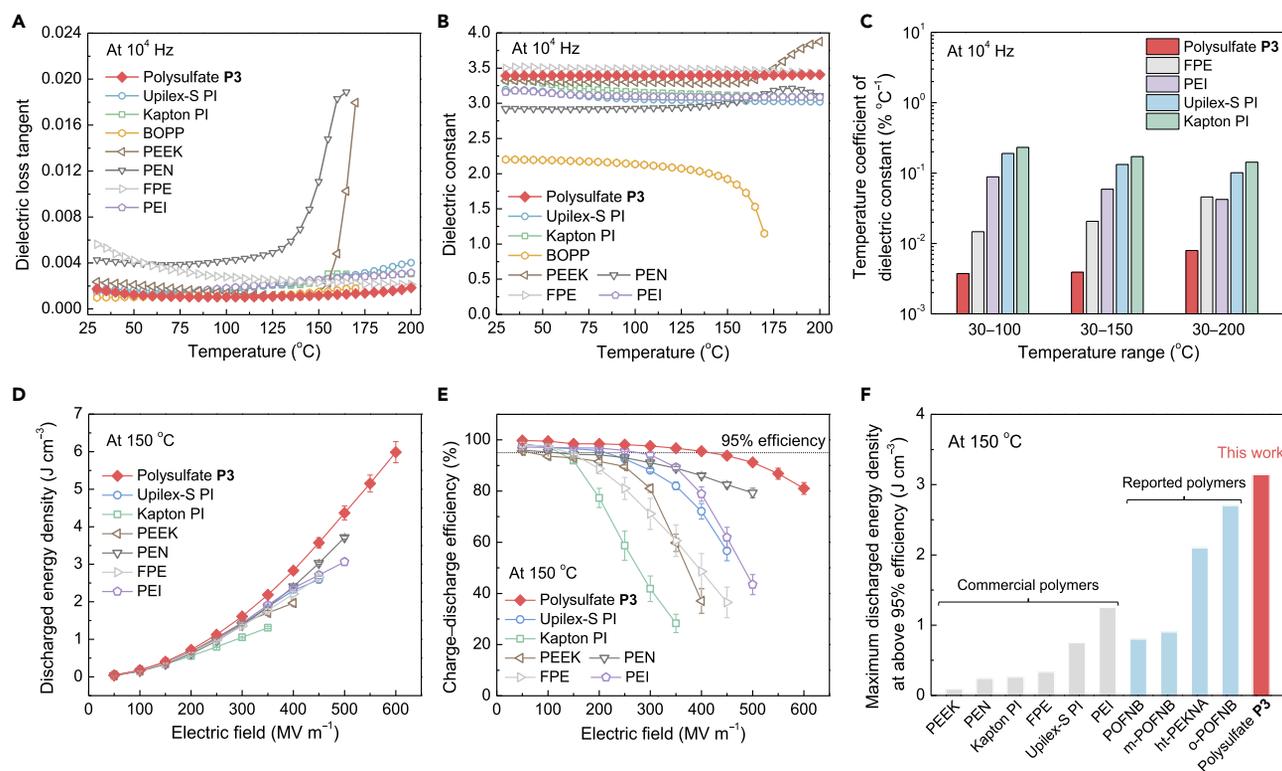
Figure 2. Dielectric properties and electrostatic energy storage performance

(A and B) Temperature-dependent dielectric spectra of dielectric loss tangent (tan δ) (A) and dielectric constant (k) (B) of polysulfate **P3** and commercial dielectric polymers obtained at 10^4 Hz.

(C–E) (C) Temperature coefficient (C_T) of the dielectric constant of polysulfate **P3** and commercial dielectric polymers at various temperature ranges obtained at 10^4 Hz. Discharged energy density (U_d) (D) and charge-discharge efficiency (η) (E) of polysulfate **P3** and commercial dielectric polymers measured at 150°C. Error bars show standard deviation obtained from at least three measurements using different samples.

(F) Maximum U_d at above 95% η of polysulfate **P3**, commercial dielectric polymers, and the state-of-the-art reported dielectric polymers at 150°C. POFNB, polyoxafluorinatednorbornene[19]; m-POFNB, meta-POFNB[24]; o-POFNB, ortho-POFNB[23]; ht-PEKNA, heat-treated poly(naphthalene ether ketone amide).[39]

backbone. The rigid aromatic subunits are responsible for lowering the backbone motions, while the sulfate linkers can absorb the friction energy between rigid aromatic segments, leading to suppressed dielectric loss.[20,22] Molecular dynamics (MDs) simulations (Figure S13) provide further support that the slopes of the mean square displacement (MSD) curve of the polysulfates are among the smallest in comparison with other control aromatic polymers. In addition, the k of polysulfate **P3** remains remarkably stable at ~3.4 across a wide temperature range from 30°C to 200°C, corresponding to a temperature coefficient (C_T, see experimental procedures) of 0.008% °C^{-1}, the smallest when compared with FPE, PEI, Upilex-S PI, and Kapton PI measured at the same temperature range (Figure 2C), and also lower than that of the state-of-the-art high-temperature dielectric polymer polyoxafluorinatednorbornene[19] (POFNB, C_T of 0.016% °C^{-1} for the temperature range 20°C–180°C) and the dielectric nanocomposites of c-BCB/Al$_2$O$_3$ nanoplates[40] and c-BCB/BN nanosheets[4] (C_Ts of ~0.023% °C^{-1} and ~0.025% °C^{-1}, respectively, for the temperature range 30°C–200°C) (c-BCB, crosslinked divinyltetramethyldisiloxane bis(benzocyclobutene)).

We then measured the E_b of the polysulfates at various temperatures. A two-parameter Weibull distribution function (see experimental procedures) has been utilized to

assess the experimental results, as shown in Figures S14 and S15 and Table S3. All polymers deliver an ultrahigh Weibull E_b ($\geq$650 MV m^{-1}) at 25°C and show a typical drop in E_b with temperature. In comparison with polysulfates P1 and P2, polysulfate P3 with the highest T_g exhibits the highest Weibull E_b at elevated temperatures. For instance, at 125°C and 150°C, the Weibull E_b of polysulfate P3 is 664 and 604 MV m^{-1}, respectively, compared with 617 and 488 MV m^{-1} of the polysulfate P2 with the second-best T_g. In contrast, polysulfate P1 delivers a notably reduced Weibull E_b of 366 MV m^{-1} at 125°C, which is limited by T_g to withstand higher temperatures. At the same time, the thickness dependence of E_b is demonstrated using polysulfate P3 films with various thicknesses (Figure S16), where only minor variation (<3%) of Weibull E_b has been observed across the investigated thickness range of 2–14 μm. To be consistent with the thickness of BOPP films used in commercial dielectric capacitors (i.e., ~3 μm),[38] the thickness of the free-standing polysulfate films is carefully controlled to be around 2–5 μm in the rest of this work.

The electrostatic energy storage capability of polysulfate-based capacitors has also been evaluated. The U_d and η values are derived from unipolar electric displacement-electric field (D-E) loops, as illustrated in Figures S17–S19. At 25°C, all the polysulfates show high η values >93% over the entire applied electric field range up to 750 MV m^{-1}. The U_d at the same electric field follows the rank of P2 > P1 > P3 (e.g., at 400 MV m^{-1}, 3.09, 2.86, 2.79 J cm^{-3} for P2, P1, and P3, respectively), which is in line with the descending trend of k (i.e., 3.80, 3.53, and 3.40 for P2, P1, and P3, respectively) (Figures 1B and S20). At elevated temperatures reaching 150°C and above, the polysulfate P3 maintains the greatest capacitive performance among the three polysulfates (Figures S21 and S22), thanks to its highest T_g and Weibull E_b coupled with the relatively high k. P3 also outperforms all the known high-T_g dielectric polymers at 150°C in terms of the U_d and the η (Figures 2D and 2E). For example, at 150°C, polysulfate P3 can discharge an U_d of ~6 J cm^{-3} under 600 MV m^{-1} with an η of higher than 80%. Comparatively, PEN and PEI, the next-best dielectric polymers evaluated in this study, deliver a U_d of 3.71 and 3.06 J cm^{-3} along with a η of 79.2% and 43.5%, respectively, at their maximum tolerable field of 500 MV m^{-1}. A low η implicates a substantial portion of the charged energy that is converted into waste heat, which reduces the operational reliability and lifespan of capacitors. We summarized the U_d achieved at above 95% η and under 150°C in Figure 2F, in which the polysulfate P3 stands out from both the commercially available capacitor films and the latest reported dielectric polymers.[19,23,24,39] For instance, with less than 5% energy loss during their charge and discharge processes, the maximum U_d values of polysulfate P3 is 3.14 J cm^{-3}, comparing favorably with ~2.7 J cm^{-3} of ortho-polyoxafluorinatednorbornene (o-POFNB), ~2.1 J cm^{-3} of heat-treated poly(naphthalene ether ketone amide) (ht-PEKNA), and 1.25 J cm^{-3} of PEI, while other polymers display U_ds < 1 J cm^{-3}.

Surface coating of ultrathin Al$_2$O$_3$ layers on polymer films

The excellent baseline dielectric and energy storage properties of polysulfates encouraged further property optimization by nanodielectric engineering. Nanofiller doping has been widely adopted at the lab scale to enhance the electrostatic energy storage performance of polymers,[41–45] though the scalability remains dubious due to the complication arising from mixing and dispersion. Surface coating processes based on surface self-assembly, physical vapor deposition (PVD), and chemical vapor deposition (CVD) offer more controllable alternatives.[46–49] Atomic layer deposition (ALD), a special branch of CVD that grows the target material layer-by-layer with atomic level homogeneity, stands out as an attractive gas phase deposition method on account of its programmable coating thickness and easy processability under
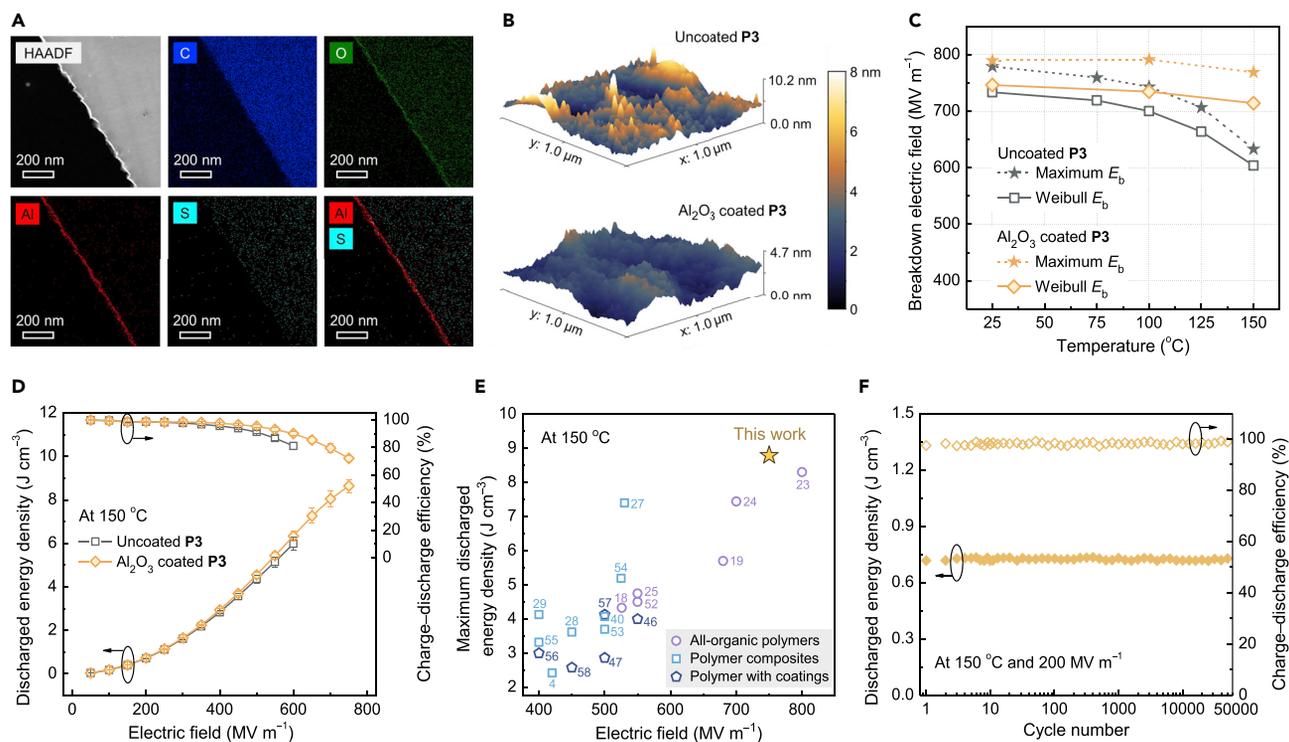
Figure 3. Atomic layer deposition for enhancing performance

(A) Cross-sectional STEM high-angle annular dark-field (HAADF) image and EDS mapping of C, O, Al, and S of a ~5.1 nm Al_2O_3 coated polysulfate **P3** film.

(B) AFM surface topography of uncoated polysulfate **P3** and ~5.1 nm Al_2O_3 coated **P3** films.

(C) Temperature-dependent breakdown electric field of uncoated polysulfate **P3** and ~5.1 nm Al_2O_3 coated **P3** films.

(D) Discharged energy density (U_d) and charge-discharge efficiency (η) of uncoated polysulfate **P3** and ~5.1 nm Al_2O_3 coated **P3** films measured at 150°C. Error bars show standard deviation obtained from at least three measurements using different samples.

(E) Performance comparison of the maximum discharged energy density among ~5.1 nm Al_2O_3 coated polysulfate **P3** and other reported free-standing dielectric polymeric films at 150°C. All-organic polymers include PEI-, VK-, PNFA-, and POFNB-based materials[18,19,23–25,52]; polymer composites include PEI-, PI-, and BCB-based materials[4,27–29,40,53–55]; polymer with coatings include PEI- and PI-based materials.[46,47,56–58] (PEI, polyetherimide; VK, poly(chlorotrifluoroethylene-*co*-vinylidene fluoride); PNFA, poly(arylene ether amide); POFNB, polyoxafluorinatednorbornene; PI, polyimide; BCB, divinyltetramethyldisiloxane bis(benzocyclobutene)).

(F) Charging/discharging cyclic test results of ~5.1 nm Al_2O_3 coated polysulfate **P3** film measured at 150°C and 200 MV m^{-1}.

relatively low temperatures when compared with conventional PVD and CVD technologies.[50,51] Here, we demonstrate the substantial improvement of high-temperature dielectric and energy storage properties by introducing ultrathin wide band-gap Al_2O_3 nanocoatings onto both sides of the polysulfate **P3** films via plasma-assisted ALD (see experimental procedures and Figures S23 and S24). The thickness of the Al_2O_3 nanocoatings could be readily regulated from ~1.8 to 168 nm by varying deposition cycles and was confirmed by scanning transmission electron microscopic (STEM) imaging in conjunction with energy-dispersive spectroscopy (EDS) mapping analysis (Figure 3A, S25, and S26), from which the inorganic layers can be well distinguished according to the elemental distribution of C, O, Al and S. The conformal deposition of the Al_2O_3 layers was verified by atomic force microscopy (AFM) (Figures 3B and S27). The root mean square (RMS) roughness of the coating layers, ranging between 0.8 and 2.7 nm, is comparable to that of the pristine solution-cast polymer film. Such conformal coating is advantageous not only for facilitating the subsequent metallization[48] but also for alleviating local electric field distortion to ensure high insulation strength.[59]

We first investigated the influence of the coating thickness on the E_b of the polysulfate P3 films (Figure S28; Table S4). The Weibull E_b of the polysulfate P3 films peaks at ~5 nm of Al_2O_3 coating, i.e., 714 MV m^{-1} at 150°C, amounting to an 18% improvement over the uncoated polysulfate P3. The optimized coating thickness also induces a higher β value derived from Weibull statistics, i.e., 17.2 for the Al_2O_3 coated sample versus 13.4 for the neat polymer, denoting a narrower distribution of experimental results and improved dielectric reliability of the surface-coated films. To understand the correlation between the thickness of Al_2O_3 layer and the insulating strength of the dielectric films, we considered three coating models for excessively thin, optimized, and thicker layers, respectively (Figure S29). The effect of layer thickness is attributed to the interplay of the following two factors: injection barrier introduction and defect accumulation. The former associates with the polymer-Al_2O_3 interface that plays a key role in impeding charge injection, which is more effective when the deposited coatings are optimally thin (e.g., ~5 nm in this study), ideally defect-free, and can be further interpreted using the "thin layer strengthening theory" proposed by Seitz.[60] This is also supported by reports in semiconductor gate oxides where electrons in <10 nm layers undergo ballistic transport, thus limiting impact ionization.[61,62] When the coating layer is excessively thin (e.g., ≤2–3 nm), the tunneling effect cannot be ignored,[63] which invalidates the injection barrier imposed by the Al_2O_3 layer and leads to large tunneling current. On the other hand, defects are likely to accumulate in thicker Al_2O_3 layers (e.g., >20 nm) due to the incomplete chemisorption of trimethyl aluminum at low temperature,[64,65] amounting to detrimental effects that are unfavorable for electrical insulation (e.g., lowering E_b, U_d and η; increasing leakage current) of polysulfate P3 films. Nonetheless, it is noteworthy that the whole deposition process is performed under a low temperature of ≤40°C. The annealing-free feature is of crucial practical significance to fully retain the physicochemical properties of the plain polymer from being affected under heat treatment.

We then focused on comparing the E_b of ~5 nm Al_2O_3 coated and uncoated polysulfate P3 films at varying temperatures (Figure S30; Table S5). Although both films show a downward trend in E_b with increasing temperature, better retained E_b values are found at elevated temperatures upon the incorporation of an Al_2O_3 nanocoating (Figure 3C). For instance, the Weibull E_b values decrease by 17.6% for uncoated polysulfate P3 but only by 4.3% for the ~5 nm Al_2O_3-coated sample from 25 to 150°C. More specifically, at 25°C, the Al_2O_3-coated film shows limited enhancement of U_d and η compared with the neat polysulfate P3, while the difference is more pronounced at elevated temperatures up to 150°C (Figures S31 and S32), suggesting that Al_2O_3 nanocoatings effectively enhance the thermo-dielectric stability.

We successively assessed the energy storage properties of Al_2O_3-coated polysulfate P3 films at 150°C (Figures S33–S35). The slimmest D-E loop (i.e., the highest η) is achieved for the polymer film with the ~5 nm Al_2O_3 coating for all films tested under the same electric field, which matches well with the variations seen in Weibull E_b evaluations. Notably, the optimal coating thickness in our study is more than an order of magnitude smaller than that of conventional inorganic oxide coatings adopted for polymeric capacitor films. For comparison, Table S6 surveys recent noteworthy works employing oxide coatings for free-standing dielectric polymer films, where the thinnest coating is ~80 nm.[46–48,56,66,67] To prove whether it may be general that the few-nanometer thickness is optimal for higher performance, PEN, which has been identified as one of the best commodity capacitor-grade films in our earlier assessment, was selected as the control polymer system. It is evident that the highest Weibull E_b value is reached with coating layers of Al_2O_3 as thin as ~5.6 nm

(Figure S36; Table S7), further indicating a critical yet overlooked sub-10 nm size region that has both fundamental and practical implications for polymer dielectrics. From a practical standpoint, ALD is unfavorable for fabricating thick coatings due to the extended deposition time. However, this work demonstrates the need for ultrathin coatings, which transforms ALD into a more viable option for the large-scale processing of dielectric films. The ultrathin coatings achieved under low processing temperature engenders additional benefits such as higher throughput, benign fabrication process, and better retained mechanical flexibility and operational cyclability of polymer films, all conducive to future wound capacitor cell fabrication. As demonstrated by the $\sim$5 nm Al_2O_3 coated polysulfate **P3** samples, such ALD deposition slightly increases the Young's modulus and tensile strength, and well retains the stretchability of the films (Figure S37; Table S8). In addition, the ultrathin coating has negligible influence on the low-field dielectric properties (i.e., k and tan δ) of **P3** films over the entire range of frequency and temperature (Figure S38).

Equipped with concurrently improved η and E_b, the polysulfate **P3** film with the optimal Al_2O_3 coating thickness delivers a maximal U_d of 8.64 J cm^{-3} at 150°C, which represents a 24% enhancement compared with the uncoated film (Figure 3D). To the best of our knowledge, this U_d is the highest among free-standing dielectric polymer and nanocomposite thin films operated at the same temperature,[4,18,19,23–25,28,29,40,46,47,52–58] as summarized in Figure 3E and Table S9. Besides U_d, the Al_2O_3 coated **P3** film also exhibits better or comparable U_d values at efficiencies above 90% or 95% when compared against literature results at 150°C (Figure S39; Table S10). At an applied field of 200 MV m^{-1}, which is the working condition of capacitors in common power systems such as hybrid EVs,[18] the Al_2O_3-coated polysulfate **P3** film shows almost negligible energy loss (i.e., <2% at 150°C) and considerably higher U_d and power density than those of the benchmark BOPP (e.g., $\sim$0.72 J cm^{-3} and 19.22 MW L^{-1} at 150°C vs. $\sim$0.4 J cm^{-3} and 10.08 MW L^{-1} at 105°C) (Figures S40 and S41). Both uncoated and coated polysulfate **P3** films retain capacitive performance (data variation < 1.6%) over successive 50,000 charging/discharging cycles at 200 MV m^{-1} and 150°C (Figures 3F, S42, and S43), and also show marginal differences in the Weibull statistics of E_b values after performing cyclic bending tests (Figures S44 and S45). Encouragingly, a self-clearing behavior toward electrical damage has been demonstrated in polysulfate **P3**-based film capacitor devices at 150°C. When a dielectric breakdown event occurred in the film device during the first D-E loop cycle, the device could still withstand the electric field in the following cycles with only slight decreases in U_d and η values (Figure S46). Top view scanning electron microscopic (SEM) image coupled with EDS mappings uncover that an area with vaporized electrodes has been formed around the breakdown hole, which is isolated with no continuous Au and C element distributions detected (Figure S47), corroborating the self-clearing behavior.[15] These results verify that the polysulfate-based dielectric films exhibit favorable operational reliability and are suitable for flexible electronic applications.

Electrical conduction and charge behavior

To gain a more insightful understanding of the coating-induced improvement of high-temperature capacitive performance, we performed leakage current measurements of polysulfate **P3**-based films since it is well recognized that electrical conduction is the foremost energy loss mechanism of dielectric materials at elevated electric fields. The leakage current density of thin films measured at 150°C and 200 MV m^{-1} declines as thin layers of the Al_2O_3 coating were applied (Figure S48). It reaches a minimum at the optimal coating thickness of $\sim$5 nm, with a decrease of over an order of magnitude compared with that of the neat polymer. The coating thickness dependence on current density is also the result of the counterbalance between the
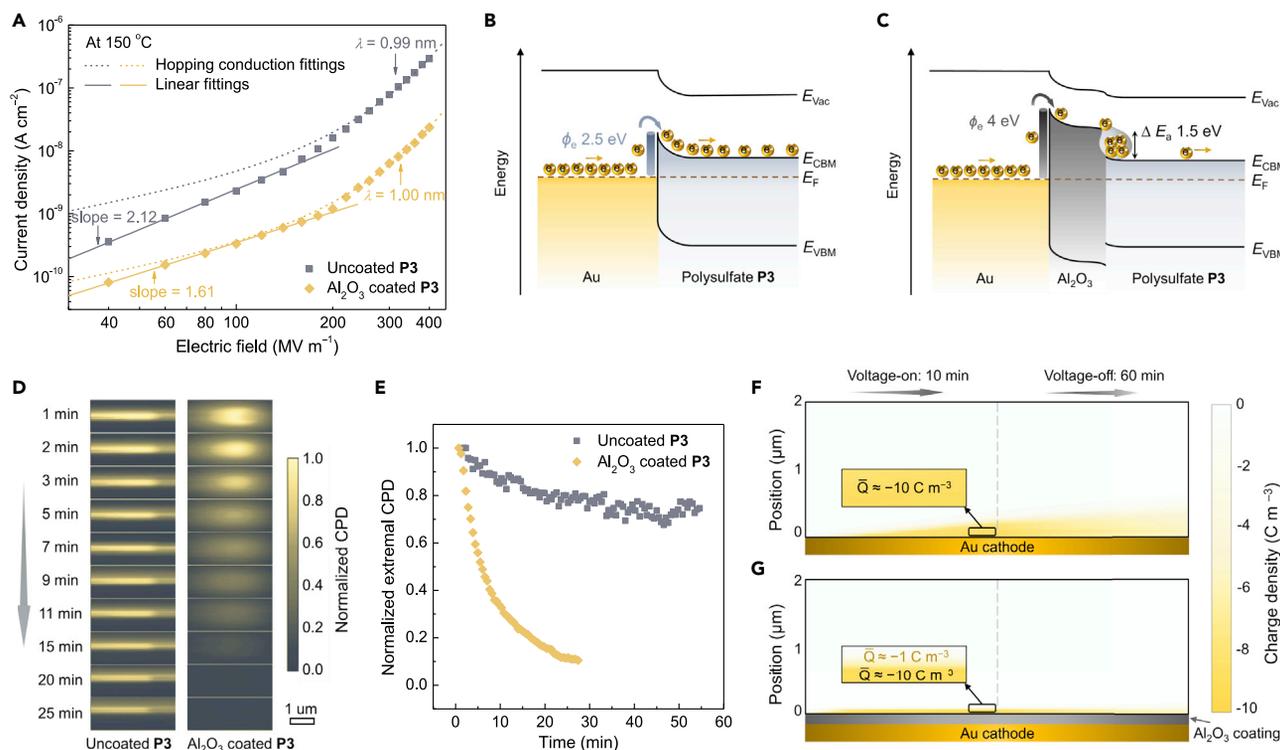
Figure 4. Electrical conduction and charge transport behavior

(A–C) (A) Segmented fittings of leakage current density versus electric field of uncoated polysulfate **P3** and ∼5.1 nm Al_2O_3-coated **P3** films measured at 150°C. Dashed curves represent fittings to hyperbolic sine. Solid curves represent linear fittings. Energy band diagrams at the electrode Au-polysulfate **P3** interface (B) and the dual interfaces of electrode Au-Al_2O_3 and Al_2O_3-polysulfate **P3** (C). φ_e is the electron barrier height, ΔE_a is the electron affinity difference between two dielectric materials, E_{Vac} is the vacuum level, E_{CBM} is the conduction band minimum, E_F is the Fermi level, and E_{VBM} is the valence band maximum.

(D) KPFM maps of the normalized extremal contact potential difference (CPD) of uncoated polysulfate **P3** and ∼5.1 nm Al_2O_3-coated **P3** films. From top to bottom, ∼1, ∼2, ∼3, ∼5, ∼7, ∼9, ∼11, ∼15, ∼20, and ∼25 min after applying an 85 V voltage at the center of the samples.

(E–G) (E) Decay of the normalized extremal CPD over time of uncoated polysulfate **P3** and ∼5.1 nm Al_2O_3 coated **P3** films. BCT simulations representing charge transport behavior during voltage-on (10 min) and voltage-off (60 min), including charge distribution and average charge density ($\overline{Q}$) near the electrode-dielectric interfaces of the native polysulfate **P3** model (F) and the Al_2O_3 coated **P3** model (G).

formation of charge barrier and the accumulation of defects, which shows an inverse correlation to the trends in Weibull E_b, U_d, and η results, as expected. Field-dependent leakage current density studies reveal a distinct transition for both the native and Al_2O_3-coated polysulfate **P3** films within the field strength range of 40–400 MV m^{-1} (Figure 4A). While the electrical conduction in dielectrics is known as a complicated process and is synergically affected by various mechanisms such as the Ohmic, space-charge-limited, and hopping conductions as well as Poole-Frenkel and Schottky emissions,[15,25,68] the segmented fittings suggest that the conduction behavior in polysulfate **P3** films is primarily dominated by charge injection-governed Schottky emission in the low-field region (i.e., ≤200 MV m^{-1}) and a transport-limited hopping process in the higher field region, respectively (Figures S49–S51). The Al_2O_3 nanocoating decreases the slope of the low-field linear fitting curve (s) but has almost no effect on the hopping distances (λ, ∼1 nm) derived from fitted hyperbolic sines based on a hopping conduction model (see experimental procedures and Figure 4A). The results indicate that the ultrathin Al_2O_3 layer mainly regulates charge injection near the interface between the electrodes and the dielectric material.

The nanocoating improved electrical insulating behavior can be rationalized based on the corresponding energy band diagrams of the electrode-dielectric interfaces,

the band structures of which were derived from X-ray photoelectron spectroscopy (XPS) and ultraviolet photoelectron spectroscopy (UPS) (Figures 4B, 4C, and S52–S55). As a result of a smaller electron affinity (E_a) and a larger E_g of Al_2O_3 relative to polysulfate P3, the interfacial barrier heights for electrons and holes are raised from 2.5 and 1.4 eV for the Au-polymer interface to 4.0 and 2.7 eV for the Au-Al_2O_3 interface, respectively, which account for the inhibited Schottky emission observed in Figure S40. Another considerable energy barrier (ΔE_a =1.5 eV) is present in the heterojunction of Al_2O_3-polysulfate P3, which can act as interfacial trap sites[25,28] and has been further elucidated by tracking the surface potential decay using the non-contact Kelvin probe force microscopy (KPFM) (see experimental procedures; Figures 4D and S56). In the coated polysulfate P3 film, the Al_2O_3 layer leads to a remarkably faster charge dissipation, with the normalized extremal contact potential difference (CPD) declining dramatically within 5 min. In stark contrast, the normalized extremal CPD of the coating-free film shows minor decay even after 50 min. As compared in Figure 4E, the peak value of the normalized CPD decreases to ~10% for the coated film while retaining over 80% for the uncoated sample at 25 min. The contrasting charge dissipation behavior between different interfaces supports that the injected charges migrate across the coating layer (during voltage-on) and accumulate at the Al_2O_3-polymer interface, which induces a built-in electric field in the opposite direction to the applied field[25] (Figure S57). Such a reverse electric field provides a driving force for charges to rapidly dissipate in the Al_2O_3 coated sample during voltage-off (i.e., KPFM scanning). The presence of the built-in field near the Al_2O_3-polymer interface also contributes to an augmented injection barrier, which is expected to repel further net inflow of electrons from the electrode. Since the direct KPFM detection of potential distribution along the film cross-section requires precise sectioning with ideal surface flatness, which is challenging and limited by the sample fabrication, we employed numerical simulation based on a modified bipolar charge transport (BCT) model to gain further insight into the charge injection process (see experimental procedures and Figures S58–S61). As shown in Figures 4F–4G, with the application of an electric field of 200 MV m^{-1} at 150°C, the charge injection is more restrained in the Al_2O_3-coated polymer than that in the uncoated polymer. Without Al_2O_3, the calculated dissipation region of the injected charge is more than 0.5 μm apart from the electrode, in contrast to less than 0.2 μm for the Al_2O_3 coated polymer. Additionally, the average charge density ($\overline{Q}$) is well suppressed due to the inorganic coating, e.g., reduced by ~ten times at the region 0.2 μm inward the electrode, compared with the native polymer. These results demonstrate that the interface-induced injection barrier is responsible for the reduction in the leakage current and for the synergetic increases in E_b, U_d, and η observed in the Al_2O_3 coated polysulfate films, confirming the critical role of nanocoatings in improving the polymer's dielectric and energy storage characteristics.

Conclusions

We have unraveled the exceptional potential of the readily accessible aryloxy linked polysulfates as an emerging class of high-temperature, high-dielectric-strength polymers to fulfill the stringent requirements for harsh electrification conditions. The specific fluorene core-based polysulfate P3 balances key operational considerations regarding electronic, electrical, and thermal parameters for high-temperature polymer dielectrics, displaying a wide band gap, high glass transition temperature, high dielectric constant, and low dielectric loss. The corresponding thin films have demonstrated excellent dielectric properties over a wide temperature range from room temperature to 150°C. Furthermore, the deposition of ultrathin (~5 nm) Al_2O_3 nanocoatings by an ALD process leads to significantly reduced leakage current,

and consequently further improved breakdown strength and electrostatic energy storage capacities. The resulting film capacitors deliver a high discharged energy density of 8.64 J cm^{-3} at 150°C, outperforming the state-of-the-art dielectric polymers and nanocomposites. Key insights into the correlation between dielectric properties and charge transport behavior illuminate the critical role of the coating layer at the relevant thickness (a few nanometers) in enhancing the high-temperature electrostatic energy storage performance of polymeric films. The facile and scalable click chemistry-enabled polymer syntheses, coupled with the straightforward fabrication process, set the stage for further structure-property relationship screens of diverse SuFEx-related monomers. The aim is to locate materials able to deliver robust electrification in the face of even fiercer temperatures and electric fields.

EXPERIMENTAL PROCEDURES

Resource availability

Lead contact
Further information and request for resources and materials should be directed to and will be fulfilled by the lead contact, Yi Liu (yliu@lbl.gov).

Materials availability
This study did not generate new unique materials.

Data and code availability
The data and code presented in this work are available from the corresponding authors upon reasonable request.

Polymeric film preparation
Polysulfates **P1–P3** were synthesized by bifluoride-catalyzed SuFEx polycondensation (2 mol % of potassium bifluoride [KHF$_2$]/1 mol % of 18-crown-6 catalysis in NMP at 130°C) according to a previous procedure.[34] **P1** powders were dissolved in NMP to yield a clear solution with a concentration of 20 mg mL^{-1} under magnetic mechanical stirring overnight at 60°C. **P2** and **P3** powders were dissolved in DMF to yield a clear solution with a concentration of 20 mg mL^{-1} under magnetic mechanical stirring overnight at room temperature. The obtained **P1**/NMP solution was cast on clean glass slides at room temperature and kept in an air-circulating oven at 95°C for 12 h to evaporate the solvent. The obtained **P2**/DMF and **P3**/DMF solutions were cast on clean glass slides at room temperature and kept in an air-circulating oven at 65°C for 12 h to evaporate the solvent. Afterward, the resultant polymer films were peeled off in deionized water and placed in a vacuum oven at 180°C for 12 h to remove water and solvent residuals. The typical thickness of the free-standing polysulfate films is 2–5 μm. The other two series of polysulfate **P3** films with different thicknesses of 9.1–10 and 12.8–14 μm were prepared by the same casting method using larger amounts of **P3**/DMF solution, which are exclusively utilized in the thickness-dependent breakdown studies. Other free-standing polymer films of Upilex-S PI, Kapton PI, BOPP, PEEK, PEN, FPE, and PEI were obtained from PolyK Technologies, USA. The details of these commercial capacitor-grade dielectric films can be found in Table S2.

Al$_2$O$_3$ coatings were deposited using plasma-assisted ALD at 40°C (FLEXAL, Oxford Instruments). At each cycle, trimethylaluminum (TMA) is dosed for 20 ms, followed by TMA purge using Ar/O$_2$ mixture for 4 s and plasma dose for 2 s. All processes were conducted at 15 mTorr. The deposition rate was controlled at 0.139 nm per cycle. The polymer films were suspended using a custom steel frame to ensure equal depositions on both sides. For all the dielectric and electrical measurements, both

sides of the polymeric films were coated with gold electrodes using a magnetron sputter (Q150R, Quorum) with a thickness of ∼20 nm and an area of 4 mm^2 for dielectric breakdown and electric displacement-electric field (D-E) loop measurements, an area of 28.26 mm^2 for direct fast discharge (power density) test, and an area of 50.24 mm^2 for dielectric spectroscopy, leakage current and cyclic charging/discharging measurements.

Structural characterization

UV-vis absorption spectra of the polymer film samples were obtained on an Agilent Cary 5000 UV-vis-NIR spectrometer. The optical transmittance of the samples was measured in the wavelength range 200–700 nm. AFM images were acquired with an Asylum Research Cypher VES atomic force microscope in a nitrogen saturated atmosphere. In order to resolve the samples topography, AFM images were obtained using the Amplitude Modulation technique. KPFM, images were acquired with an Asylum Research Cypher VES atomic force microscope in a nitrogen saturated atmosphere. Free-standing polymeric film samples were attached onto indium tin oxide (ITO)-coated glass substrates (2–3 Ω sq^{-1}, Thin Film Devices, USA), silver paint (Leit-silber 200, TED PELLA, USA) was used to ensure electrical contact between the polymeric film and ITO layer, as well as electrically ground the ITO layer. For KPFM images, a low-frequency electrostatic excitation (∼2 kHz) is applied on the metallized AFM tip (PPP-EFM from NanoWorld with typical stiffness ∼2 N m^{-1} and resonance frequency ∼70 kHz). A feedback loop controls an additional DC voltage applied to the tip in order to keep the electrostatic tip-sample interaction as small as possible. This applied DC voltage provides a direct measure of the contact potential difference (CPD) between the tip and the sample. For charge injection, a typical conductive-AFM setup was used with a high-voltage source being connected to the tip and the back of the sample. A voltage ramp is applied from 0 to 85 V at a rate of 15 V s^{-1} and then kept at 85 V for 5 s before turning it off.

Transmission electron microscope (TEM) images were obtained using a FEI Tecnai 12 at an accelerating voltage of 120 kV. Scanning transmission electron microscope in conjunction with energy-dispersive X-ray spectroscopy (STEM-EDS) was performed at National Center for Electron Microscopy (NCEM) at the Molecular Foundry of the Lawrence Berkeley National Laboratory by using a FEI TitanX 60-300 microscope operated at 200 kV. The Bruker windowless EDS detector with a solid angle of 0.7 steradians enables high count rates with minimal dead time. The data were visualized with Esprit 1.9. Cross-sectional samples for TEM, and STEM-EDS measurements were prepared by embedding polymeric film samples in epoxy resin (Araldite 502, Electron Microscopy Sciences) and cured at 60°C overnight. Sections about 60 nm in thickness were microtomed using an RMC MT-X Ultramicrotome (Boeckler Instruments), floated on top of the water, and picked up on copper TEM grids.

Electrical characterization

Dielectric spectra of the polymeric film samples were acquired over wide frequency and temperature ranges using a Hewlett Packard 4284A LCR meter. The samples in a dielectric test fixture were placed in a temperature chamber (EC1A, Sun Electronic Systems), where the temperature-dependent dielectric spectra were acquired between 30°C and 200°C. The temperature coefficient C_T of the k is obtained from Equation 1

$$C_T = \left| \frac{k_i - k_0}{T_i - T_0} \right| \times 100\%, \qquad \text{(Equation 1)}$$

where k_i is the k at temperature T_i, and k_0 is the k at T_0 (i.e., 30°C). Dielectric breakdown strengths of the polymeric film samples were measured using a Trek 610D instrument amplifier as the voltage source based on an electrostatic pull-down method, where a DC voltage ramp of 500 V s^{-1} was applied to the film samples until dielectric failure. The breakdown strength was evaluated by performing a two-parameter Weibull distribution analysis (Equation 2) on at least 10 samples

$$P(E_b) = 1 - \exp\left(-\left(\frac{E_b}{\alpha}\right)^\beta\right), \qquad \text{(Equation 2)}$$

where $P(E_b)$ is the probability of breakdown at a certain electric field strength, E_b is the measured dielectric breakdown field, α is the Weibull breakdown strength (i.e., Weibull E_b) which is associated with the electric field at a 63.2% probability of breakdown, β is the shape parameter which represents the dispersion degree of the data. D-E loops of the polymeric film samples were measured under varied applied electric fields using a modified Sawyer-Tower circuit, which is integrated with a PK-CPE1801 high-voltage test system (PolyK Technologies). The voltages with a unipolar triangular waveform were applied at a frequency of 100 Hz. The cyclic charging/discharging measurements were performed by collecting D-E loops under a consecutive repeated electric field of 200 MV m^{-1} based on the same high-voltage test system using the Fatigue mode. The direct fast discharge tests were performed through a capacitor discharge system with a high-voltage metal oxide semiconductor field-effect transistor (MOSFET) switch (Behlke HTS81). The charged energy was released to a load resistor (R_L), the resistance of the R_L was selected as 100 kΩ. For dielectric breakdown, D-E loop and fast discharge measurements, the samples were immersed in Galden HT-270 PFPE fluorinated fluid to avoid creeping discharge, and the temperature was controlled using a digital hot plate equipped with a thermal couple. Leakage current densities of the polymeric film samples were acquired under varied applied electric field strengths in a temperature chamber (EC1A, Sun Electronic Systems), using a Keithley 6514 electrometer coupled with an external Trek 610D amplifier as the voltage source. According to the hopping conduction equation, leakage current density (J) is given as

$$J(E, T) = 2ne\lambda v \times \exp\left(-\frac{W_a}{K_B T}\right) \times \sinh\left(\frac{\lambda eE}{2K_B T}\right), \qquad \text{(Equation 3)}$$

where E is the applied electric field during current density measurement, n is the carrier concentration, λ is the hopping distance, v is the attempt-to-escape frequency, W_a is the activation energy, T is the temperature, e is the charge of the carriers, and K_B is the Boltzmann's constant. Equation 3 can be simplified as

$$J(E) = A * \sinh(B \times E), \qquad \text{(Equation 4)}$$

where A and B are two lumped parameters.

Simulations

DFT calculations were carried out using Material Studio (Accelrys.) according to the Cambridge Sequential Total Energy Package (CASTEP) approach. The geometry optimization and the density of states (DOS) calculation were completed by employing a plane-wave basis set, the Hybrid Functional Becke3LYP (B3LYP). MD calculations were conducted through Material Studio (Accelrys) using the FORCITE module with a force field of condensed-phase optimized molecular potentials for atomistic simulation studies (COMPASSs). MSDs were calculated through 10 ns of isovolumetric-isothermal ensemble (NVT with fixed particle number N, volume V, and temperature T). Numerical simulations were based on a modified BCT model, which considers charge generation, extraction, migration, trapping, detrapping, and recombination processes. The parameters for BCT model simulation can be found in Table S11. Finite element method (FEM)

in COMSOL MULTIPHYSICS was used for equation solving. Multi-physical filed coupling of the electrostatics (ESs) model and transport of diluted species (TDS) model were applied to illustrate the transport process of charges.

SUPPLEMENTAL INFORMATION

Supplemental information can be found online at https://doi.org/10.1016/j.joule.2022.12.010.

AUTHOR CONTRIBUTIONS

Y.L., P.W., K.B.S., and H.L. conceived the idea. Y.L. and H.L. designed the experiments. H.K. and B.G. conducted polymer synthesis under the supervision of K.B.S. and P.W. H.L. and B.S.C. prepared device samples for measurements under the supervision of Y.L., R.R., and A.M.S. H.L., C.Y., and S.W.S. carried out electrical, thermal, and optical measurements under the supervision of Y.L. Z.X., and Tianlei Xu performed all simulations under the supervision of Z.P. A.L. conducted AFM and KPFM studies under the supervision of M.S. L.M. carried out TEM and STEM-EDS studies under the supervision of Ting Xu. J.K. carried out mechanical testing under the supervision of R.O.R. and Ting Xu. H.L. and V.A. carried out SEM-EDS studies. L.M.K. and V.A. performed XPS and UPS measurements. Y.L., H.L., Z.X., B.S.C., A.L., and H.K. analyzed the data. Y.L., K.B.S., and H.L. wrote the manuscript with help from P.W., Z.X. and B.S.C. all authors discussed the results and provided inputs to the manuscript.

DECLARATION OF INTERESTS

A patent application (serial no. 63/420,407) covering this work has been filed.

INCLUSION AND DIVERSITY

We support inclusive, diverse and equitable conduct of research.

REFERENCES

1. Johnson, R.W., Evans, J.L., Jacobsen, P., Thompson, J.R.R., and Christopher, M. (2004). The changing automotive environment: high-temperature electronics. IEEE Trans. Electron. Packag. Manuf. *27*, 164–176. https://doi.org/10.1109/TEPM.2004.843109.

2. Watson, J., and Castro, G. (2015). A review of high-temperature electronics technology and applications. J. Mater. Sci: Mater. Electron. *26*, 9226–9235. https://doi.org/10.1007/s10854-015-3459-4.

3. Buttay, C., Planson, D., Allard, B., Bergogne, D., Bevilacqua, P., Joubert, C., Lazar, M., Martin, C., Morel, H., Tournier, D., and Raynaud, C. (2011). State of the art of high temperature power electronics. Mater. Sci. Eng. B *176*, 283–288. https://doi.org/10.1016/j.mseb.2010.10.003.

4. Li, Q., Chen, L., Gadinski, M.R., Zhang, S., Zhang, G., Li, H.U., et al. (2015). Flexible high-temperature dielectric materials from polymer nanocomposites. Nature *523*, 576–579. https://doi.org/10.1038/nature14647.

5. Chu, B., Zhou, X., Ren, K., Neese, B., Lin, M., Wang, Q., Bauer, F., and Zhang, Q.M. (2006). A dielectric polymer with high electric energy density and fast discharge speed. Science *313*, 334–336. https://doi.org/10.1126/science.1127798.

6. Feng, Y., Hasegawa, Y., Suga, T., Nishide, H., Yang, L., Chen, G., and Li, S. (2019). Tuning conformational H-bonding arrays in aromatic/alicyclic polythiourea toward high energy-storable dielectric material. Macromolecules *52*, 8781–8787. https://doi.org/10.1021/acs.macromol.9b01785.

7. Prateek, Thakur, V.K., and Gupta, R.K. (2016). Recent progress on ferroelectric polymer-based nanocomposites for high energy density capacitors: synthesis, dielectric properties, and future aspects. Chem. Rev. *116*, 4260–4317. https://doi.org/10.1021/acs.chemrev.5b00495.

8. Meng, N., Ren, X., Santagiuliana, G., Ventura, L., Zhang, H., Wu, J., Yan, H., Reece, M.J., and Bilotti, E. (2019). Ultrahigh β-phase content poly(vinylidene fluoride) with relaxor-like ferroelectricity for high energy density capacitors. Nat. Commun. *10*, 4535. https://doi.org/10.1038/s41467-019-12391-3.

9. Chen, Q., Shen, Y., Zhang, S., and Zhang, Q.M. (2015). Polymer-based dielectrics with high energy storage density. Annu. Rev. Mater. Res. *45*, 433–458. https://doi.org/10.1146/annurev-matsci-070214-021017.

10. Cheng, R., Wang, Y., Men, R., Lei, Z., Song, J., Li, Y., and Guo, M. (2022). High-energy-density polymer dielectrics via compositional and structural tailoring for electrical energy storage. iScience *25*, 104837. https://doi.org/10.1016/j.isci.2022.104837.

11. Singh, M., Apata, I.E., Samant, S., Wu, W., Tawade, B.V., Pradhan, N., Raghavan, D., and Karim, A. (2022). Nanoscale strategies to enhance the energy storage capacity of polymeric dielectric capacitors: review of recent advances. Polym. Rev. *62*, 211–260. https://doi.org/10.1080/15583724.2021.1917609.

12. Wang, G., Lu, Z., Li, Y., Li, L., Ji, H., Feteira, A., Zhou, D., Wang, D., Zhang, S., and Reaney, I.M.

(2021). Electroceramics for high-energy density capacitors: current status and future perspectives. Chem. Rev. *121*, 6124–6172. https://doi.org/10.1021/acs.chemrev.0c01264.

13. Pan, H., Li, F., Liu, Y., Zhang, Q., Wang, M., Lan, S., Zheng, Y., Ma, J., Gu, L., Shen, Y., et al. (2019). Ultrahigh–energy density lead-free dielectric films via polymorphic nanodomain design. Science *365*, 578–582. https://doi.org/10.1126/science.aaw8109.

14. Jian, X.D., Chen, X., and Zhang, Q.M. (2019). Relaxor ferroelectric capacitors embrace polymorphic nanodomains. Joule *3*, 2296–2298. https://doi.org/10.1016/j.joule.2019.09.008.

15. Li, H., Zhou, Y., Liu, Y., Li, L., Liu, Y., and Wang, Q. (2021). Dielectric polymers for high-temperature capacitive energy storage. Chem. Soc. Rev. *50*, 6369–6400. https://doi.org/10.1039/D0CS00765J.

16. Liu, X.-J., Zheng, M.-S., Chen, G., Dang, Z.-M., and Zha, J.-W. (2022). High-temperature polyimide dielectric materials for energy storage: theory, design, preparation and properties. Energy Environ. Sci. *15*, 56–81. https://doi.org/10.1039/D1EE03186D.

17. Li, Q., Yao, F.-Z., Liu, Y., Zhang, G., Wang, H., and Wang, Q. (2018). High-temperature dielectric materials for electrical energy storage. Annu. Rev. Mater. Res. *48*, 219–243. https://doi.org/10.1146/annurev-matsci-070317-124435.

18. Li, H., Gadinski, M.R., Huang, Y., Ren, L., Zhou, Y., Ai, D., Han, Z., Yao, B., and Wang, Q. (2020). Crosslinked fluoropolymers exhibiting superior high-temperature energy density and charge–discharge efficiency. Energy Environ. Sci. *13*, 1279–1286. https://doi.org/10.1039/C9EE03603B.

19. Wu, C., Deshmukh, A.A., Li, Z., Chen, L., Alamri, A., Wang, Y., et al. (2020). Flexible temperature-invariant polymer dielectrics with large bandgap. Adv. Mater. *32*, 2000499. https://doi.org/10.1002/adma.202000499.

20. Zhang, Z., Zheng, J., Premasiri, K., Kwok, M.-H., Li, Q., Li, R., Zhang, S., Litt, M.H., Gao, X.P.A., and Zhu, L. (2020). High-κ polymers of intrinsic microporosity: a new class of high temperature and low loss dielectrics for printed electronics. Mater. Horiz. *7*, 592–597. https://doi.org/10.1039/C9MH01261C.

21. Zhang, Z., Wang, D.H., Litt, M.H., Tan, L.S., and Zhu, L. (2018). High-temperature and high-energy-density dipolar glass polymers based on sulfonylated poly(2, 6-dimethyl-1, 4-phenylene oxide). Angew. Chem. Int. Ed. Engl. *57*, 1528–1531. https://doi.org/10.1002/anie.201710474.

22. Wei, J., and Zhu, L. (2020). Intrinsic polymer dielectrics for high energy density and low loss electric energy storage. Prog. Polym. Sci. *106*, 101254. https://doi.org/10.1016/j.progpolymsci.2020.101254.

23. Deshmukh, A.A., Wu, C., Yassin, O., Mishra, A., Chen, L., Alamri, A., Li, Z., Zhou, J., Mutlu, Z., Sotzing, M., et al. (2022). Flexible polyolefin dielectric by strategic design of organic modules for harsh condition electrification.

Energy Environ. Sci. *15*, 1307–1314. https://doi.org/10.1039/D1EE02630E.

24. Wu, C., Deshmukh, A.A., Yassin, O., Zhou, J., Alamri, A., Vellek, J., Shukla, S., Sotzing, M., Casalini, R., Sotzing, G.A., and Cao, Y. (2021). Flexible cyclic-olefin with enhanced dipolar relaxation for harsh condition electrification. Proc. Natl. Acad. Sci. USA *118*. e2115367118. https://doi.org/10.1073/pnas.2115367118.

25. Yuan, C., Zhou, Y., Zhu, Y., Liang, J., Wang, S., Peng, S., Li, Y., Cheng, S., Yang, M., Hu, J., et al. (2020). Polymer/molecular semiconductor all-organic composites for high-temperature dielectric energy storage. Nat. Commun. *11*, 3919. https://doi.org/10.1038/s41467-020-17760-x.

26. Zhang, Q., Chen, X., Zhang, B., Zhang, T., Lu, W., Chen, Z., Liu, Z., Kim, S.H., Donovan, B., Warzoha, R.J., et al. (2021). High-temperature polymers with record-high breakdown strength enabled by rationally designed chain-packing behavior in blends. Matter *4*, 2448–2459. https://doi.org/10.1016/j.matt.2021.04.026.

27. Dai, Z., Bao, Z., Ding, S., Liu, C., Sun, H., Wang, H., et al. (2022). Scalable polyimide-poly(amic acid) copolymer based nanocomposites for high-temperature capacitive energy storage. Adv. Mater. *34*, 2101976. https://doi.org/10.1002/adma.202101976.

28. Dong, J., Hu, R., Niu, Y., Sun, L., Li, L., Li, S., Pan, D., Xu, X., Gong, R., Cheng, J., et al. (2022). Enhancing high-temperature capacitor performance of polymer nanocomposites by adjusting the energy level structure in the micro-/meso-scopic interface region. Nano Energy *99*, 107314. https://doi.org/10.1016/j.nanoen.2022.107314.

29. Li, Q., Liu, F., Yang, T., Gadinski, M.R., Zhang, G., Chen, L.-Q., and Wang, Q. (2016). Sandwich-structured polymer nanocomposites with high energy density and great charge–discharge efficiency at elevated temperatures. Proc. Natl. Acad. Sci. USA *113*, 9995–10000. https://doi.org/10.1073/pnas.1603792113.

30. Wu, C., Deshmukh, A.A., Chen, L., Ramprasad, R., Sotzing, G.A., and Cao, Y. (2022). Rational design of all-organic flexible high-temperature polymer dielectrics. Matter *5*, 2615–2623. https://doi.org/10.1016/j.matt.2022.06.064.

31. Stalke, D. (2021). Chapter 2. Chemical concepts of bonding and current research problems, or: why should we bother to engage in chemical bonding analysis? In Complementary Bonding Analysis, S. Grabowsky, ed. (De Gruyter), pp. 9–40.

32. Dong, J., Krasnova, L., Finn, M.G., and Sharpless, K.B. (2014). Sulfur(VI) fluoride exchange (SuFEx): another good reaction for click chemistry. Angew. Chem. Int. Ed. Engl. *53*, 9430–9448. https://doi.org/10.1002/anie.201309399.

33. Dong, J., Sharpless, K.B., Kwisnek, L., Oakdale, J.S., and Fokin, V.V. (2014). SuFEx-based synthesis of polysulfates. Angew. Chem. Int. Ed. Engl. *53*, 9466–9470. https://doi.org/10.1002/anie.201403758.

34. Gao, B., Zhang, L., Zheng, Q., Zhou, F., Klivansky, L.M., Lu, J., Liu, Y., Dong, J., Wu, P., and Sharpless, K.B. (2017). Bifluoride-catalysed sulfur (VI) fluoride exchange reaction for the synthesis of polysulfates and polysulfonates.

Nat. Chem. 9, 1083–1088. https://doi.org/10.1038/nchem.2796.

35. Li, S., Li, G., Gao, B., Pujari, S.P., Chen, X., Kim, H., Zhou, F., Klivansky, L.M., Liu, Y., Driss, H., et al. (2021). SuFExable polymers with helical structures derived from thionyl tetrafluoride. Nat. Chem. 13, 858–867. https://doi.org/10.1038/s41557-021-00726-x.

36. Geng, Z., Shin, J.J., Xi, Y., and Hawker, C.J. (2021). Click chemistry strategies for the accelerated synthesis of functional macromolecules. J. Polym. Sci. 59, 963–1042. https://doi.org/10.1002/pol.20210126.

37. Kolb, H.C., Finn, M.G., and Sharpless, K.B. (2001). Click chemistry: diverse chemical function from a few good reactions. Angew. Chem. Int. Ed. Engl. 40, 2004–2021. https://doi.org/10.1002/1521-3773(20010601)40:11<2004::AID-ANIE2004>3.0.CO;2-5.

38. Zhang, G., Li, Q., Allahyarov, E., Li, Y., and Zhu, L. (2021). Challenges and opportunities of polymer nanodielectrics for capacitive energy storage. ACS Appl. Mater. Interfaces 13, 37939–37960. https://doi.org/10.1021/acsami.1c04991.

39. Xu, D., Xu, W., Seery, T., Zhang, H., Zhou, C., Pang, J., Zhang, Y., and Jiang, Z. (2020). Rational design of soluble polyaramid for high-efficiency energy storage dielectric materials at elevated temperatures. Macromol. Mater. Eng. 305, 1900820. https://doi.org/10.1002/mame.201900820.

40. Li, H., Ai, D., Ren, L., Yao, B., Han, Z., Shen, Z., et al. (2019). Scalable polymer nanocomposites with record high-temperature capacitive performance enabled by rationally designed nanostructured inorganic fillers. Adv. Mater. 31, 1900875. https://doi.org/10.1002/adma.201900875.

41. Guo, N., DiBenedetto, S.A., Tewari, P., Lanagan, M.T., Ratner, M.A., and Marks, T.J. (2010). Nanoparticle, size, shape, and interfacial effects on leakage current density, permittivity, and breakdown strength of metal oxide–polyolefin nanocomposites: experiment and theory. Chem. Mater. 22, 1567–1578. https://doi.org/10.1021/cm902852h.

42. Chen, J., Shen, Z., Kang, Q., Qian, X., Li, S., Jiang, P., and Huang, X. (2022). Chemical adsorption on 2D dielectric nanosheets for matrix free nanocomposites with ultrahigh electrical energy storage. Sci. Bull. 67, 609–618. https://doi.org/10.1016/j.scib.2021.10.011.

43. Luo, H., Zhou, X., Ellingford, C., Zhang, Y., Chen, S., Zhou, K., Zhang, D., Bowen, C.R., and Wan, C. (2019). Interface design for high energy density polymer nanocomposites. Chem. Soc. Rev. 48, 4424–4465. https://doi.org/10.1039/C9CS00043G.

44. Luo, S., Yu, J., Yu, S., Sun, R., Cao, L., Liao, W.H., and Wong, C.P. (2019). Significantly enhanced electrostatic energy storage performance of flexible polymer composites by introducing highly insulating-ferroelectric microhybrids as fillers. Adv. Energy Mater. 9, 1803204. https://doi.org/10.1002/aenm.201803204.

45. Pan, Z., Yao, L., Zhai, J., Yao, X., and Chen, H. (2018). Interfacial coupling effect in organic/inorganic nanocomposites with high energy density. Adv. Mater. 30, 1705662. https://doi.org/10.1002/adma.201705662.

46. Cheng, S., Zhou, Y., Li, Y., Yuan, C., Yang, M., Fu, J., Hu, J., He, J., and Li, Q. (2021). Polymer dielectrics sandwiched by medium-dielectric-constant nanoscale deposition layers for high-temperature capacitive energy storage. Energy Storage Mater. 42, 445–453. https://doi.org/10.1016/j.ensm.2021.07.018.

47. Zhou, Y., Li, Q., Dang, B., Yang, Y., Shao, T., Li, H., et al. (2018). A scalable, high-throughput, and environmentally benign approach to polymer dielectrics exhibiting significantly improved capacitive performance at high temperatures. Adv. Mater. 30, 1805672. https://doi.org/10.1002/adma.201805672.

48. Wu, X., Liu, Y., Lin, X., Huang, E., Song, G., and Tan, D.Q. (2022). Atomic layer deposition coated polymer films with enhanced high-temperature dielectric strength suitable for film capacitors. Surf. Interfaces 28, 101686. https://doi.org/10.1016/j.surfin.2021.101686.

49. Wu, C., LaChance, A.M., Baferani, M.A., Shen, K., Li, Z., Hou, Z., Wang, N., Wang, Y., Sun, L., and Cao, Y. (2022). Scalable self-assembly interfacial engineering for high temperature dielectric energy storage. iScience 25, 104601. https://doi.org/10.1016/j.isci.2022.104601.

50. Song, G., and Tan, D.Q. (2020). Atomic layer deposition for polypropylene film engineering—a review. Macromol. Mater. Eng. 305, 2000127. https://doi.org/10.1002/mame.202000127.

51. Oviroh, P.O., Akbarzadeh, R., Pan, D., Coetzee, R.A.M., and Jen, T.C. (2019). New development of atomic layer deposition: processes, methods and applications. Sci. Technol. Adv. Mater. 20, 465–496. https://doi.org/10.1080/14686996.2019.1599694.

52. Zhou, C., Xu, W., Zhang, B., Zhang, Y., Shen, C., Xu, Q., Liu, X., Bertram, F., Bernholc, J., Jiang, Z., et al. (2022). Curly-packed structure polymers for high-temperature capacitive energy storage. Chem. Mater. 34, 2333–2341. https://doi.org/10.1021/acs.chemmater.1c04220.

53. Fan, M., Hu, P., Dan, Z., Jiang, J., Sun, B., and Shen, Y. (2020). Significantly increased energy density and discharge efficiency at high temperature in polyetherimide nanocomposites by a small amount of Al_2O_3 nanoparticles. J. Mater. Chem. A 8, 24536–24542. https://doi.org/10.1039/D0TA08908G.

54. Ren, L., Li, H., Xie, Z., Ai, D., Zhou, Y., Liu, Y., Zhang, S., Yang, L., Zhao, X., Peng, Z., et al. (2021). High-temperature high-energy-density dielectric polymer nanocomposites utilizing inorganic core–shell nanostructured nanofillers. Adv. Energy Mater. 11, 2101297. https://doi.org/10.1002/aenm.202101297.

55. Ren, W., Pan, J., Dan, Z., Zhang, T., Jiang, J., Fan, M., Hu, P., Li, M., Lin, Y., Nan, C.-W., and Shen, Y. (2021). High-temperature electrical energy storage performances of dipolar glass polymer nanocomposites filled with trace ultrafine nanoparticles. Chem. Eng. J. 420, 127614. https://doi.org/10.1016/j.cej.2020.127614.

56. Dong, J., Hu, R., Xu, X., Chen, J., Niu, Y., Wang, F., Hao, J., Wu, K., Wang, Q., and Wang, H. (2021). A facile in situ surface-functionalization approach to scalable laminated high-temperature polymer dielectrics with ultrahigh capacitive performance. Adv. Funct. Mater. 31, 2102644. https://doi.org/10.1002/adfm.202102644.

57. Zhang, T., Yang, L., Zhang, C., Feng, Y., Wang, J., Shen, Z., Chen, Q., Lei, Q., and Chi, Q. (2022). Polymer dielectric films exhibiting superior high-temperature capacitive performance by utilizing an inorganic insulation interlayer. Mater. Horiz. 9, 1273–1282. https://doi.org/10.1039/D1MH01918J.

58. Azizi, A., Gadinski, M.R., Li, Q., AlSaud, M.A., Wang, J., Wang, Y., Wang, B., Liu, F., Chen, L.Q., Alem, N., and Wang, Q. (2017). High-performance polymers sandwiched with chemical vapor deposited hexagonal boron nitrides as scalable high-temperature dielectric materials. Adv. Mater. 29, 1701864. https://doi.org/10.1002/adma.201701864.

59. Pei, J.-Y., Zhong, S.-L., Zhao, Y., Yin, L.-J., Feng, Q.-K., Huang, L., Liu, D.-F., Zhang, Y.-X., and Dang, Z.-M. (2021). All-organic dielectric polymer films exhibiting superior electric breakdown strength and discharged energy density by adjusting the electrode–dielectric interface with an organic nano-interlayer. Energy Environ. Sci. 14, 5513–5522. https://doi.org/10.1039/D1EE01960K.

60. Seitz, F. (1949). On the theory of electron multiplication in crystals. Phys. Rev. 76, 1376–1393. https://doi.org/10.1103/PhysRev.76.1376.

61. Lombardo, S., Stathis, J.H., Linder, B.P., Pey, K.L., Palumbo, F., and Tung, C.H. (2005). Dielectric breakdown mechanisms in gate oxides. J. Appl. Phys. 98, 121301. https://doi.org/10.1063/1.2147714.

62. DiMaria, D.J. (1997). Defect production, degradation, and breakdown of silicon dioxide films. Solid State Electron. 41, 957–965. https://doi.org/10.1016/S0038-1101(97)00006-3.

63. Groner, M.D., Elam, J.W., Fabreguette, F.H., and George, S.M. (2002). Electrical characterization of thin Al_2O_3 films grown by atomic layer deposition on silicon and various metal substrates. Thin Solid Films 413, 186–197. https://doi.org/10.1016/S0040-6090(02)00438-8.

64. Groner, M.D., Fabreguette, F.H., Elam, J.W., and George, S.M. (2004). Low-temperature Al_2O_3 atomic layer deposition. Chem. Mater. 16, 639–645. https://doi.org/10.1021/cm0304546.

65. Heil, S.B.S., Kudlacek, P., Langereis, E., Engeln, R., van de Sanden, M.C.M., and Kessels, W.M.M. (2006). In situ reaction mechanism studies of plasma-assisted atomic layer deposition of Al_2O_3. Appl. Phys. Lett. 89, 131505. https://doi.org/10.1063/1.2357886.

66. Wu, X., Song, G., Zhang, X., Lin, X., Ivry, Y., and Tan, D.Q. (2022). Multilayer polyetherimide films incorporating alumina nanolayers for dielectric capacitors. Chem. Eng. J. 450, 137940. https://doi.org/10.1016/j.cej.2022.137940.

67. Liu, G., Lei, Q., Feng, Y., Zhang, C., Zhang, T., Chen, Q., and Chi, Q. (2022). High-temperature energy storage dielectric with inhibition of carrier injection/migration based on band structure regulation. InfoMat, e12368. https://doi.org/10.1002/inf2.12368.

68. Chiu, F.C. (2014). A review on conduction mechanisms in dielectric films. Adv. Mater. Sci. Eng. 2014, 1–18. https://doi.org/10.1155/2014/578168.